

The first results of monitoring observations of a meteor echo at ISTP SB RAS EKB radar: algorithms, validation, statistics

Fedorov R.R. Bergardt O.I.

November 16, 2021

Abstract

The paper presents the implementation of algorithms for automatic search for signals scattered at meteor tracks based on the ISTP SB RAS EKB radar data. The algorithm is divided into two phases - the detection of a meteoric echo and the determination of its parameters. In general, the algorithm is similar to the algorithms used for specialized meteor radars, but uses direct fitting of received signal quadrature components by a model when finding the parameters of meteor trail. Based on the analysis of maximum of the Geminid meteor shower 13.12.2016 the aspect sensitivity of the scattered signals detected by the algorithm was shown. This proves that the detected signals correspond to scattering by irregularities elongated with the direction to the radiant of the meteor shower. This also confirms that the source of signals detected by the algorithm are meteor traces. In this paper, we solve the inverse problem of reconstructing the vector of the neutral wind velocity from the radar data by the weighted least-squares technique. A comparison of the roses of horizontal neutral winds obtained in the model of two-dimensional (horizontal) wind and three-dimensional wind is made. Their similarity is shown and expected predominance of the zonal component over the meridional one is shown too. The implemented algorithm allows us to process the scattered signals in the real time. The detection algorithm has started its continuous operation at the ISTP SB RAS EKB radar at the end of 2016. Keywords: meteor trail echo, decameter radar

1 Introduction

The study of meteor showers is currently one of the tasks of investigating asteroid-comet hazards. The study of meteor showers and individual meteors makes it possible to investigate the relationship of meteor showers with parental bodies (asteroids and comets) and thereby study the statistics and dynamics of small bodies in the solar system. In application to the physics of the upper atmosphere, meteors are more likely the sources of disturbances in the atmosphere, and allow one to investigate the processes of generation of small-scale irregularities, as well as their dynamics caused by the background processes in the upper atmosphere. One of the most common ways to use meteors to monitor the upper atmosphere is to study the neutral wind velocity. The burning of meteors occurs

at altitudes of about 60-100 km, and lower, depending on the meteoroid mass [Briczinski et al.(2009)]. The processes taking place from glow and ionization (for small meteors) to the electrophone effects and shock waves (for large bolides) are variable and complex [Janches et al.(2009), Berngardt et al.(2013)], and are widely studied [Zhu et al.(2016)]. The most massive meteoroids can burn partially, reaching the Earth's surface. Smaller meteors burn in the atmosphere nearly completely, allowing us to estimate the mass of the meteoroid based on the burn dynamics.

Radar observations are one of the most common techniques for observing meteors. In radar observations, two types of scattered signal are identified based on the scattering object nature: the scattering by the burning body (head-echo) and scattering by the meteor trail (trail-echo).

Scattering on the meteoroid body is more isotropic. The scattering cross section is smaller than the cross section for scattering on a meteor trail. Due to this the studies of the head-echo requires high potential radars. These radars include MU radar[Kero et al.(2012)], ALTAIR[Close et al.(2002)], and some of the incoherent scatter radars (Millstone-Hill[Erickson et al.(2001)], EISCAT[Szasz et al.(2008)], Arecibo[Mathews et al.(2003)]). One of the problems solved by the studies is meteor trajectory investigations, allowing one to study meteor showers and their sources. In this case, it is possible to find the trajectory directly, as well as to calculate the velocity of meteoroid entry into the atmosphere, and to calculate the deceleration rate of the body[Szasz et al.(2008), Mathews et al.(2003), Mathews et al.(2010)]. Joining these data together allows one to estimate the mass of a meteoroid and the direction to the radiant.

Another way to find the radiant of meteor shower is the use of trail scattering and aspect sensitivity of the meteor trail [Lovell(1954), Campbell-Brown(2008), Jones et al.(2005)]. The meteor trace is the elongated irregularity of electron density in the lower ionosphere at heights 60-100 km. Due to this the scattered signal power is aspect-sensitive and has maximum when radar line-of-sight is perpendicular to meteor trail (illustrated at Fig.1A)[McKinley(1961)]. Therefore the use of trail scattering requires a relatively low radar potential and very common in regular studies.

By the ratio between the plasma frequency in the meteor trail and the sounding frequency, the meteor trails are traditionally divided into underdense and overdense ones. Less massive meteoroids correspond to underdense trails, and more massive meteoroids produce overdense trails.

Obviously, that less massive meteors prevail over more massive ones. Therefore the underdense echo is often used in different practical tasks, for example for studying the dynamics of the upper atmosphere. The trail formed after the combustion of a meteor is an ionized region that recombines under the action of the ambipolar diffusion [Jones and Jones(1990)] and the electron density in the trail decreases over time. As a result, the scattering of the signal at the underdense trail is characterized by a specific exponential decay of the scattered signal power. The time of decay is related with the diffusion coefficient, and this allows researchers to measure this coefficient directly. In addition, the track is in a dense atmosphere and therefore, is carried away by a neutral wind at an appropriate altitude due to electron-neutral collisions. This allows one to measure the dynamics of neutral wind at the meteor trail altitudes [Nakamura et al.(1991), Hall et al.(2006)]. The use of dense networks of instruments, such as meteor radar networks[Deegan et al.(1970)] or SuperDARN

radar network [Hall et al.(1997)], allows researchers to study the motions in the upper atmosphere in a large spatial region in the monitoring mode.

An important part of meteor studies is the algorithms for automatic signal detection and for estimating meteor trail parameters. Algorithms for interpreting the trail-echo usually analyze the power of the received signal, search for sharp peaks in power with an exponential decay specific for underdense echo [Tsutsumi et al.(1999)]. Detection of meteor trail echoes at SuperDARN radar is performed by various algorithms: by studying the average correlation characteristics of the scattered signal [Jenkins and Jarvis(1999)], by analyzing the shape of the scattered single-pulse signal with the high frequency discretization [Parris(2003)], or by analyzing the scattered signal from complex sounding sequences [Yukimatu and Tsutsumi(2003)].

In this paper we describe the implementation of algorithms for automatic search for meteors at ISTP SB RAS EKB radar. Also we validate the algorithm by using the aspect sensitivity of scattered signals. We present the first statistics of meteor trails observations at the radar. Also we describe a method for solving the inverse problem of reconstructing the vector of the neutral wind velocity from the obtained data without elevation angle information.

2 EKB ISTP SB RAS radar

The EKB ISTP SB RAS radar is a decameter over-the-horizon radar, developed and manufactured at the University of Leicester (UK) and similar to the SuperDARN radars. The radar is located in the Sverdlovsk Region of the Russian Federation (56.5 N, 58.5 E). Its field of view has an azimuthal width of about 52° and is divided into 16 directions (beams) $3^\circ - 6^\circ$ width each depending on the sounding frequency. The central direction of the radar field of view has the azimuth 19° from the North. The radar field-of-view and its beam configuration are shown in Fig.1B,C. The radar operates in 8-20MHz frequency range, providing a range resolution in standard modes of 15-45 km and has the maximal range about 3000-4500 km. The EKB radar is a stereo radar of CUTLASS kind and can operate at two channels (with different carrier frequencies and different beams) simultaneously. The antenna array of the EKB radar has a symmetry axis, antenna pattern has a significant back lobe in the regular frequency range of 10-12 MHz, so the surface of antenna pattern for each beam can be considered as the surface of a cone. The shapes of the antenna pattern at different beams are shown in Fig.1B (according to [Berngardt et al.(2017)]).

The standard operational mode of the radar is the transmitting of various multipulse (Golomb) sequences [Berngardt et al.(2015)], which provide high spatial and spectral resolution simultaneously. Standard autocorrelation processing of the signal and the accumulation of the autocorrelation function over the 4-8 seconds for each selected beam, as well as the subsequent analysis of the amplitude-phase structure of the averaged autocorrelation function by algorithms specially developed by SuperDARN community [Ribeiro et al.(2013)], makes it possible to estimate the average characteristics of scattered ionospheric signals, as well as signals scattered from the Earth's surface.

The most common way of processing the meteor echo at SuperDARN radars is the analysis of the average autocorrelation functions: power, range, line-of-sight Doppler velocity and spectral width. The meteor trail detection algorithms

are based on the statistical thresholds of these parameters determined experimentally in joint measurements with meteor radars. The time resolution of these techniques corresponds to the accumulation time of the autocorrelation function and is usually about 4-8 seconds [Arnold et al.(2003)].

3 Algorithm of meteor trail detection and estimation of its parameters

3.1 Basic description of the algorithm

As it was stated earlier, standard measurements by the radar are carried out with complex multi-pulse sounding sequences. This allows us to treat the radar as a meteor radar with 0.3 msec sounding pulse and with an irregular pulse repetition rate. Time resolution of the radar changes from 2.4 msec (minimal interpulse interval) to about 36 msec (maximal interpulse interval). The registration of the full shape scattered signal (quadrature components) is started after the beginning of each sounding sequence with standard temporal discretization rate 0.3 msec, which provides 45 km range resolution of the measurements.

The optimal way of analysing meteor trail scattering is to search for and to determine the parameters of the scattered signal simultaneously to improve the algorithm accuracy. However, the need of the real-time data processing, demanding computer resources and limited computing resources at the radar did not allow us to implement the most accurate technique for trail detection and estimation of its parameters. Therefore the problem was divided into two tasks, solved separately: task 1 - meteor trail detection and estimating of the distance to the scatterer; task 2 - fitting the model of the trail scattered signal to the data and estimation of the its parameters. The meteor trail detection was carried out by the amplitude of the scattered signal, and model fit and estimation of its parameters was carried out by the analysis of full structure of the scattered signal (its quadrature components).

3.2 Task 1 - meteor trail detection

The task of the detection stage is to search for bursts of signal amplitude that are potentially suitable for interpretation as a meteor trail scatter. The radar registers the quadrature components of the scattered signal. After transfer to zero carrier frequency (heterodyning) it can be described as a complex signal $u(t)$:

$$u(t) = I(t) + iQ(t) = A(t)e^{i\varphi(t)} \quad (1)$$

where $I(t), Q(t)$ - quadrature components of the scattered signal, $A(t)$ - absolute value of the signal amplitude ('amplitude'), $\varphi(t)$ - signal phase.

Since the radar transmits a repeating complex pulse sequence, it is convenient to represent the amplitude of the scattered signal $A(t) = |u(t)|$ as a function of two arguments - the transmit moment of the nearest pulse T_m^e and the radar delay R . Here and after the bottom index $m = 0, 1, \dots$ denotes the index number of the pulse; the top index f ('first') marks the response corresponding to the first pulse of the sequence, the top index e marks the response from corresponding to any pulse in the sounding sequence - thus $T_m^f = T_m^e$ when

$m = s \cdot N_p$. Here $s = 0, 1, \dots; N_p$ is the number of pulses in the sequence, value of T_m^f is not defined for $m \neq sN_p$. These arguments are related to the moment of measurement of the signal t by the following equation:

$$t = T_m^e + 2R/c \quad (2)$$

Thus, we proceed from analyzing the amplitude modulus of the signal $A(t)$ and its quadrature components $I(t), Q(t)$ as a functions of absolute time, to the analysis of two-dimensional arrays $A(R, T_m^e)$ and $I(R, T_m^e), Q(R, T_m^e)$ respectively. It should be noted that due to the peculiarities of the transmitted sounding signal, which is a non-equidistant sequence of short pulses, the sequence $\{T_m^e\}$ is also not equidistant.

In order for the signal to be accepted as a candidate for meteor trail scattering, the signal must satisfy the following conditions (verification stages):

Stage 1. High amplitude of the burst Meteor trails are relatively rare, relatively shortlived and nearly stationary objects. We are interested in bursts of high amplitude, by which we can surely determine the other parameters of the meteor trail echo: its lifetime and the average line-of-sight velocity. Therefore, we search for an excess of the amplitude above the noise level. Since the meteor trails are quasistationary - within the lifetime of the trail their position (range) R does not depend on the time T_m^e , the meteor trail search can be carried out at each fixed range R independently. The search condition of the trail is a short-term amplitude exceeding of some threshold level. When searching, for each radar range R_k the threshold value M_k is calculated over the set of sounding runs N (one session corresponds to one sounding sequence). Then we select all the coordinates (R_k, T_m^f) of signals scattered from the first pulses of the sounding sequences, for which the signal amplitude exceeds the threshold level:

$$A(R_k, T_m^f) > M_k \quad (3)$$

Here M_k is the threshold level, defined as the average amplitude of signals scattered from the first pulses of the sounding sequences, averaged over the sounding runs:

$$M_k = \frac{1}{N} \sum_{m=1}^N A(R_k, T_{mN_p}^f) \quad (4)$$

All the solutions (R_k, T_m^f) , satisfying (3), are bursts of sufficiently high amplitude and pass to the next stage of analysis.

Stage 2. High spatial localization. Meteor trails are rare and highly localized spatial objects. Therefore, for each burst of the amplitude found at stage 1, we verify the fulfillment of the second condition-the spatial localization of the amplitude burst. For this, the average level at the ranges R_{k-1}, R_{k+1} around the trail range R_k should not exceed the threshold value m_k :

$$\frac{A(R_{k+1}, T_m^f) + A(R_{k-1}, T_m^f)}{2} < m_k \quad (5)$$

As the threshold value m_k , we use the median value of the amplitude of the signals scattered from each pulse of the sounding sequence:

$$m_k : \{F_A(m_k) = \frac{1}{2}\} \quad (6)$$

where $F_A(A(R_k, T_m^e))$ is an empirical distribution function of the amplitudes $A(R_k, T_m^e)$ for a fixed range R_k , $m \in [1..K]$, where K is the total number of pulses transmitted during the scan time.

All the detected bursts with coordinates (R_k, T_m^f) , satisfying (5), are spatially localized bursts of amplitude and pass to the next stage of analysis.

Step 3. Monotonic decrease of signal amplitude As already mentioned, the main feature of scattering by underdense trails is the exponential decay of the signal amplitude over the time. Therefore, when detecting a meteor trail echo by pulse sequences, we look for a series of bursts with an amplitude monotonically decreasing in time. To do this, the sequences of signals scattered by the first pulse of the probing sequence $T_{m+lN_p}^f$ are analyzed. They should follow the pairs (R_k, T_m^f) detected at the previous stage. The sequences should satisfy the condition (3) and should decrease in time (fulfillment of the condition (5) is not required in this case):

$$A(R_k, T_{m+lN_p}^f) > A(R_k, T_{m+(l+1)N_p}^f), l = 0 \dots s-1 \quad (7)$$

and form the sequence $S_{k,m,L}$ of signals scattered from each sounding pulse (hereinafter, 'the set'). The length L of the sequence is $L = s \cdot N_p$ elements, where s is the number of sounding sequences included in the set $S_{k,m,L}$:

$$S_{k,m,L} = ((R_k, T_m^e), (R_k, T_{m+1}^e), (R_k, T_{m+2}^e) \dots (R_k, T_{m+L}^e)) \quad (8)$$

The formation of the set is completed when the fulfillment is terminated of the condition (3):

$$\begin{cases} A(R_k, T_{m+sN_p}^f) > M_k \\ A(R_k, T_{m+(s+1)N_p}^f) < M_k \end{cases} \quad (9)$$

or the condition (7):

$$\begin{cases} A(R_k, T_{m+(s-1)N_p}^f) > A(R_k, T_{m+sN_p}^f) \\ A(R_k, T_{m+sN_p}^f) < A(R_k, T_{m+(s+1)N_p}^f) \end{cases} \quad (10)$$

In this approach, several sets $S_{k,m,L}$ can be generated, and each of them is processed separately later. The first point (R_k, T_m^f) of each set $S_{k,m,L}$ corresponding to the scattering of the first sounding pulse in the first sounding sequence in the set is considered to be the initial coordinates (range and initial moment) of the meteor trail. The length L of the sequence corresponds to the duration of the meteor echo found. In the current implementation of the algorithm, the same sounding sequence response can be included in several sets.

To reduce the noise in inversion stage, the scattering responses that do not satisfy the following condition are excluded from the resulting set $S_{k,m,L}$:

$$A(R_k, T_m^e) > m_k \quad (11)$$

, the total length of the set L is changed accordingly.

In Fig.2 is shown an example of a selected sequence corresponding to a meteor trail echo at a fixed radar range R_k as a function of time T_{m+i}^e .

3.3 Task 2 - estimation of meteor trail parameters

The main characteristics of underdense scattering at meteor trails are: the coordinates of the combustion point, the characteristic decay time and the line-of-sight Doppler velocity. For studying the diffusion processes in the upper atmosphere and the fine structure of the atmospheric wind it is important to know the combustion height and other spatial coordinates. EKB radar does not have the ability to determine the elevation angle for now, and therefore the height can not be determined from experimental data.

The amplitude of the signals scattered at underdense trails is monotonically decayed. The characteristic decay time is related with the recombination of the trail under the action of ambipolar diffusion and can be used for estimating the diffusion coefficient [Jones and Jones(1990)]. The meteor burns in dense layers of the atmosphere and therefore the trail moves under the influence of wind at the altitudes of combustion. Since the speed and direction of the wind can not change significantly during the existence of the echo, the Doppler shift of the phase of the signal is linear in the first approximation. This allows us to measure the wind line-of-sight velocity [Tsutsumi et al.(1999)] from the phase changes of the scattered signals.

In our algorithm each trail echo candidate, represented as set (8) with initial coordinates (R_k, T_m^f) and duration L , and satisfying the requirements (3,5,7) is used to solve the inverse problem of estimating the meteor trail characteristics.

For solving the inverse problem, we analyse the sequence of scattered signal quadrature components $I(t_i), Q(t_i)$, where t_i is determined by the moment T_m^e of the meteor echo start and by the distance R_k to it:

$$t_i = T_{m+i}^e + 2R_k/c; i = 0..L \quad (12)$$

The sequence of quadrature components $\{I(t_i), Q(t_i)\}_{i=0..L}$ is used to solve the inverse problem by searching for the parameters of the model signal that fits it best. An example of the experimental sequence is shown in the Fig.2C-D.

As a model signal, the well-known model [Parris(2003)] is used:

$$\begin{cases} u_m(t; A_0, \omega, \tau) = A_0(I_m(t; \omega, \tau) + iQ_m(t; \omega, \tau)) \\ I_m(t; \omega, \tau) = \theta(t)e^{-t/\tau} \cos(\omega t) \\ Q_m(t; \omega, \tau) = \theta(t)e^{-t/\tau} \sin(\omega t) \end{cases} \quad (13)$$

Here $A_0 = A_{0I} + iA_{0Q}$ is the initial complex-valued amplitude of the scattered signal with taking into account the initial phase; $I_m(t; \omega, \tau), Q_m(t; \omega, \tau)$ are the real and imaginary components of the model function as a functions of the time t for given values of the model parameters ω, τ ; $\theta(t)$ is the Heaviside function (a single step function). The optimal parameters of the model that should be found are: A_0 - real and imaginary components of the initial amplitude of the scattered signal, ω and τ - phase slope (cyclic frequency) and decay time, respectively.

The search for the optimal model parameters is carried out by the least squares method, and the optimal parameters (A_0, ω, τ) should provide the absolute minimum of the residual function $\Omega(A_0, \omega, \tau)$:

$$\Omega(A_0, \omega, \tau) = \sum_{i=0}^L |u(t_i) - u_m(t_i - t_0; A_0, \omega, \tau)|^2 = \min \quad (14)$$

Here, $u(t)$ is the complex-valued representation of the scattered signal (1), t_i are the moments of meteor trail scatter observations for given meteor trail; t_0 is the initial moment of meteor trail scatter observation for given meteor trail.

The minimization problem (14) is linear over the parameters A_{0I}, A_{0Q} (the parts of complex-valued parameter A_0) and is non-linear over the parameters ω, τ . Therefore to find the minimum (14) we use a direct search of parameters ω, τ over a grid of values and an analytical calculation of the optimal parameters A_{0I}, A_{0Q} at each point of the grid.

The following parameter grid is used in the search:

- for the Doppler frequency shift ω we use equidistant grid corresponding to Doppler velocities from -200 to 200 m/s in steps of 1 m/s. In the calculations, the Doppler velocity is converted to the Doppler frequency shift according to the classical formula $\omega = \frac{4\pi V}{\lambda}$, where λ -radar wavelength, V - Doppler velocity. Our choice of the limits for Doppler velocities is caused by the maximal drift velocities observed experimentally, and does not exceed the acoustic speed. The grid step is chosen 10 times more detailed than the standard velocity resolution of this radar (10 m/s) [Lester et al.(2004)];

- for the decay time we use an equidistant grid from 0.1 to 40 seconds in steps of 0.1 second. Selection of the step is related with the duration of the sounding sequence. The maximal grid value has been selected experimentally: on the one hand, based on the reasons of calculation speed, required for real time processing, on the other hand, to determine the lifetime of the most part of the observed meteor trails.

The optimal amplitude A_0 at each point of the grid ω, τ is defined as:

$$A_{0I} = \frac{\sum_{i=0}^L (I_m(t_i - t_0; \omega, \tau)I_e(t_i) + Q_m(t_i - t_0; \omega, \tau)Q_e(t_i))}{\sum_{i=0}^L (I_m^2(t_i - t_0; \omega, \tau) + Q_m^2(t_i - t_0; \omega, \tau))}$$

$$A_{0Q} = \frac{\sum_{i=0}^L (I_m(t_i - t_0; \omega, \tau)Q_e(t_i) - Q_m(t_i - t_0; \omega, \tau)I_e(t_i))}{\sum_{i=0}^L (I_m^2(t_i - t_0; \omega, \tau) + Q_m^2(t_i - t_0; \omega, \tau))}$$

where $t_0 = T_m^f + 2R_k/c$ is the initial moment of a meteor trail echo observations according to (12).

The optimal values of the parameters ($A_{0I}, A_{0Q}, \omega, \tau$) that provide the minimum of the functional (14) on the grid ω, τ are considered by us the actual parameters of the meteor trail - the complex-valued amplitude $A_0 = A_{0I} + iA_{0Q}$, Doppler frequency shift ω and trail lifetime τ .

4 Testing the algorithm

4.1 Accuracy of the signal model and the inversion technique

When retrieving the meteor trail parameters described in the previous section, the accuracy of the model and inversion technique was not taken into account. To estimate the accuracy of the model parameters, we checked the accuracy of the inversion technique based on the experimental data. For this purpose, the distribution of the error between the model and experimental data was analyzed

in terms of amplitude and phase errors separately based on EKB data during 2016.

The normalized error of the found solution in terms of the amplitude was determined from the standard deviation between the amplitude of the experimental data and the model one normalized to the maximal amplitude of the scattered signal on the meteor trail, according to the expression:

$$\sigma_{A,r}(\omega, \tau) = \frac{\sigma_A(\omega, \tau)}{|u(t_0)|}$$

where

$$\sigma_A^2(\omega, \tau) = \frac{1}{L} \sum_{i=0}^L (|u(t_i)| - |u_m(t_i; A_0, \omega, \tau)|)^2$$

-the mean-square deviation of the experimental amplitude from its model value.

The phase error of the solution was determined from the standard deviation between the experimental phase and the model one:

$$\sigma_\varphi^2(\omega, \tau) = \frac{1}{L} \sum_{i=0}^L (\arg(u(t_i)) - \arg(u_m(t_i; A_0, \omega, \tau)))^2$$

where $\arg(u)$ is the phase of the complex number u .

The distributions of $\sigma_{A,r}(\omega, \tau)$ and $\sigma_\varphi(\omega, \tau)$ are shown in Fig.3. They were calculated over the data obtained at EKB radar during maximums of 6 meteor showers from January to August 2016 (totally 16 days).

Fig.3 shows the following two qualitative threshold levels used by us for the data verification:

$$\begin{cases} \sigma_{A,r}(\omega, \tau) < 0.5 \\ \sigma_\varphi(\omega, \tau) < 0.7 \end{cases} \quad (15)$$

Within the threshold level for $\sigma_{A,r}(\omega, \tau)$ the most part of the errors is contained. The threshold level for $\sigma_\varphi(\omega, \tau)$ is chosen based on the reasons of an allowable error in determining the Doppler velocity: the threshold level of 0.7 radians/sec corresponds to the line-of-sight drift velocity about 2 m/s for 8MHz frequency. Fig.3B shows that the phase threshold level significantly reduces (by 57%) the number of signals that can be interpreted well.

As qualitative analysis shown, the use of the threshold levels allows us to increase the degree of confidence of the data obtained (by eliminating the cases when the model of scattering on a single underdense trail is inadequate to experimental data).

Examples of records that satisfy both the conditions (3,5,7) and the quality fit condition (15) are shown in Fig.4. In panels A) and C) are shown the amplitudes of the signal, in panel B) and D) are shown the phases of the signal; in panels E)-H) are shown the quadrature components of the scattered signal. The black circles in the figure represent the signal values used for fitting, the empty circles show the points that are rejected as noise by the criterion (11). The lines show the model shape with a minimal deviation of the model from the experimental data (14).

4.2 Meteor trail statistics according to EKB radar data

Fig.5 shows the statistics of meteor trail observations at EKB radar from December 2016 to August 2017. The statistics includes observations of more than 128 thousand meteors. Fig.5A shows the distribution of the meteor trails over their lifetime. From Fig.5 one can see that the most probable lifetime is about 0.6 seconds, which confirms the correctness of the selected limits for estimating it. The distribution spire at 40 seconds corresponds to meteor trails with lifetime more than 40 seconds, that are out of the grid and not determined by the algorithm. The sharp decrease of the distribution below 0.1sec is related with the peculiar properties of the detection algorithm: the use of the first pulse of the each sequence (step 1) does not allow us to determine the trail lifetimes less than the duration of the whole sounding sequence (that has the order of 0.1 sec). Fig.5B shows the distribution of the meteor trails over the line-of-sight Doppler velocity. From Fig.5B one can see that absolute value of velocity does not exceed 100 m/s. This confirms correctness of the limits of velocity search.

Fig.5C shows the distribution of the daily number of meteor trails detected. It shows that usually there are from 150 to 600 meteor trails per day, which corresponds to about 7 to 25 trails per hour. As the subsequent analysis shows, usually it is enough to estimate the hourly average neutral velocity. Fig.5D shows the distribution of meteor trails as a function of the radar range. It can be seen that the main part of the trail observations is concentrated at ranges less than 300 km. This corresponds well with the known limitation to the range used for processing meteor data at SuperDARN radars [Jenkins et al.(1998)]. Fig.5E shows the median velocity, as well as the first and third quartiles, as a function of local solar time. It can be seen that the quartiles are much wider than the amplitude of the diurnal variations of the median velocity, which indicates a high dynamics of wind changes and the complexity of its description within the framework of the quasi-isotropic velocity model. Fig.5F shows the median lifetime of the meteor trails, as a function of local solar time, as well as hourly number of meteors. One can see that the lifetime increases in the evening periods, and decreases in the morning periods. Hourly number of meteors has inverse dynamics. At present, the lifetime dynamics is difficult to unambiguously interpret, since the lifetime is a function of altitude, which can not be detected from our data.

Fig.5F shows the distribution of the number of echoes detected by the algorithm, depending on the local solar time. As one can see, the main peak corresponds to the pre-dawn hours, with the minimum at 15-17 LST. This distribution is similar to the distributions obtained by the optical methods [Lovell(1954)] and other radars [Thomas et al.(1988)]. Dynamics of hourly number of meteors can be explained by aspect sensitivity of detected meteor trails.

4.3 Aspect sensitivity of detected meteor trails

To verify the correctness of the interpretation of the scattered signal as underdense meteor trail echo we investigate the aspect character of the scattering. According to existing point of view, meteor trajectories during meteor showers is characterized by a certain point on the celestial sphere - the radiant. Radiants of most showers are accurately calculated for the day of maximum flow, and are published. Due to lower density the part of the atmosphere above the

meteor combustion height can be considered as not slowing the meteor and not disturbing its trajectory. So the meteor trail in the first approximation can be considered as linear with a known direction, and this direction can be calculated from the shower radiant. This fact is widely used at standard meteor radars for estimating shower radiant [Campbell-Brown(2008)]. The orientation of the meteor trail irregularity along the burn trajectory and aspect sensitivity of the scattering at the elongated irregularity lead to the well-known aspect sensitivity of meteor trail scattering [McKinley(1961)].

To check the aspect sensitivity of the meteor trails identified by the algorithm, we chose 13.12.2016 the day of maximum of Geminid meteor shower with a well known radiant. As a result of processing EKB radar data there are 877 reliable meteor trails were detected, with a peak value about 100-120 meteors per hour, which corresponds well to the forecast data for this shower [IMO(2015)].

For each meteor trail detected, we determine its geographic location from the measured azimuth to the meteor trail and range to it, assuming its 80km altitude. In the determined geographic point of scattering, the direction vector was calculated to the radiant of the meteor shower. Then the aspect angle between the direction to radiant and the direction from the radar to the scattering point was calculated.

Since the EKB radar did not have the ability to measure the elevation angle to the scatter during the experiment, and the antenna array has a significant back lobe, it is possible that the observation of some meteor trails occurs in the back lobe. Therefore, while estimating the aspect angle the calculations were made in two cases - in the case with meteor trail is in the back lobe of the antenna pattern, and in the case when meteor trail is in the main lobe of antenna pattern. Fig.6 shows the distributions of aspect angles for these two approximations, and for both radar channels used in the experiment: the solid line corresponds to the scattering in the main lobe of the antenna pattern, the dashed line corresponds to the scattering in the back lobe of the antenna pattern. From Fig.6 one can see that under the assumption of main lobe scattering the scattering is aspect sensitive one and most of the meteor trails are observed when the line of sight is nearly perpendicular to the direction to the radiant of the meteor shower. This proves that most of the scattered signals detected by the algorithm are indeed scattering by meteor trails, and the radar data can be used for estimating neutral wind.

5 Estimating the neutral wind

The main geophysical parameters determined from the meteor trail echo are the diffusion coefficient, determined from the echo lifetime [Jones and Jones(1990)] and the neutral wind velocity, determined from the Doppler frequency shift. In this paper we investigate only estimating the neutral wind velocity.

5.1 Using weighted least-squares method for estimation of neutral wind velocity

Since the radar field-of-view is quite wide, it is possible to formulate the problem of estimating the full vector of the neutral wind velocity under the assumption of wind isotropy within the radar field of view. Under this assumption it is possible

to determine the total vector of the neutral wind velocity by the weighted least-squares method. The weight function $W(R_i)$ will be discussed later. The use of weight function is necessary because of the absence of interferometric (elevation) measurements at EKB radar. Due to this the combustion height h_0 is fixed during calculations. At the same time, a significant error in determining the horizontal component of Doppler velocity may exist at small distances.

In the weighted least-squares method, the average wind is determined from the experimental data, providing the minimum of the residual functional:

$$\Omega(V_x, V_y, V_z) = \sum_i \left\{ W(R_i) (V_{d,i} + V_x k_{x,i} + V_y k_{y,i} + V_z k_{z,i})^2 \right\} = \min \quad (16)$$

here (V_x, V_y, V_z) are the projections of the neutral wind velocity in the local coordinate system of the i -th meteor trail, where (X, Y) plane is locally parallel to the Earth's surface in the spherical Earth approximation (X axis is directed to the North, Y axis is directed to the West, Z axis is directed vertically upwards); $k_{x,i}, k_{y,i}, k_{z,i}$ are the components of the unit vector of the line of sight direction from the radar to the scatter point recalculated in the scatter local coordinate system; R_i is the distance from the radar to the scatter, i is the index number of the meteor under study.

The problem of determining the components of a vector by the method (16) is a simple analytical problem that reduces to solving a system of three linear equations. The only problem that needs to be solved is the correct definition of the weight function $W(R_i)$. Let's define it.

According to the principles of weighted least square method, for a normal error distribution the correct weight function $W(R_i)$ should be inversely proportional to the dispersion of the corresponding summand in (16), caused by errors:

$$W(R_i) = \sigma_V^{-2}(R_i) \quad (17)$$

Thus, to determine the weight $W(R_i)$ we should estimate the variance of the velocity as a function of the distance to the scatterer.

To estimate the variance of $\sigma_V^{-2}(R_i)$, assume that the meteor's combustion height has a normal distribution with a mathematical expectation of h_0 and a standard deviation of σ_h . The geometry for the calculations is shown in Fig.7. The random i -th meteor produces the trail at a certain height $h_0 + \delta h_i$, corresponding to the elevation angle $\alpha_0(R) + \delta \alpha_i$, where R is the distance to the track.

The projection of the line-of-sight Doppler velocity V_d to the horizontal plane (X, Y) is:

$$V_{xy0} + \delta V_{xy,i} = V_d \cos(\alpha_0(R_i) + \delta \alpha_i) \quad (18)$$

where V_{xy0} is the mathematical expectation of V_{xy} , $\delta V_{xy,i}$ is the random deviation of the horizontal velocity projection, V_d is the measured line-of-sight Doppler velocity.

In the first approximation (for $|\delta h_i| \ll R_i$) from the geometric considerations shown in Fig.7, $\delta \alpha_i$ can be represented as:

$$\delta\alpha_i = \frac{\delta h_i}{R \cos(\alpha_0(R_i))} \quad (19)$$

Let's expand the right side of the (18) to the power series and discard all the terms smaller than the first order over the $\delta\alpha_i$. After consequent substitution the resulting expression for $\delta\alpha_i$ to (19) we obtain the following relationship between the variations in horizontal speed and scatterer height:

$$\frac{\delta V_{xy,i}}{V_d} = -\frac{\delta h_i}{R} \operatorname{tg}(\alpha_0(R_i)) \quad (20)$$

Since the variations in speed and height are proportional to each other, their variances are also proportional to each other:

$$\sigma_V^2 \left(\frac{\delta V_{xy}}{V_d} \right) = \left\{ \frac{\operatorname{tg}(\alpha_0(R))}{R} \right\}^2 \sigma_h^2(\delta h) \quad (21)$$

We suppose that the distribution of the combustion heights is constant within the radar field of view, so the dispersion of the scatterer heights $\sigma_h^2(\delta h)$ is also constant within field of view. Due to this, it does not affect the result of (16) and is assumed to be 1.

It should be noted that in the case of $\alpha_0(R) = 0$ (nearly horizontal observation of meteor scattering), the line of sight is in the horizontal plane and V_d is nearly equal to the horizontal velocity. So in this case an uncertainty of the combustion height in the first approximation does not lead to an uncertainty of the horizontal velocity. Thus, the expression (21) does not contradict with qualitative expectations of relation between elevation angle accuracy and velocity accuracy.

By substituting the expression for the velocity variance (21) into the expression (17), we obtain the necessary expression for the weight function (in the first approximation, valid for $R \ll R_E; h_0 \ll R$, where R_E is the Earth radius):

$$W(R) = \frac{R^2 (R^2 - h_0^2)}{h_0^2} \quad (22)$$

The obtained equation is very approximate and does not take into account spherical Earth, the exact distribution of the meteor trails over the height, and inaccurate at small distances (less than 300km), but is a first approximation in the weighted least squares method and can be used in practice.

5.2 Verification of the neutral wind estimation technique

Due to the absence in the radar field of view the active tools of monitoring neutral wind at heights of 60-100 km, there is no possibility for now to directly compare the data received by the radar with the data of other instruments. So we verify of the efficiency of the method described indirectly and check the validity of the obtained results qualitatively.

As already mentioned, the main component of the neutral wind at these altitudes is the horizontal wind, its vertical component is often neglected [Manning et al.(1954)Manning, Peterson]. In the framework of the weighted least squares method considered by us before, the average two-dimensional (horizontal) wind (V_x, V_y) can be determined from experimental data based on the minimum condition for the following residual:

$$\Omega(V_x, V_y) = \sum_i \left\{ W(R_i) (V_{d,i} + V_x k_{x,i} + V_y k_{y,i})^2 \right\} = \min \quad (23)$$

Here all the elements were discussed earlier when discussing the reconstruction technique of three-dimensional neutral wind (16,22).

We assume that if the estimated neutral winds are nearly horizontal, and the horizontal wind rose in 2D model (23) differs insignificantly from the horizontal wind rose in 3D model (16), then our technique is valid.

To verify the correspondence between the winds in the two models, the meteor data during the period 23/12/2016-03/07/2017 was analysed. During this period the algorithm detected 71219 meteor echoes. Based on the obtained data, the wind velocity vector was calculated in 2D model (23,22) and 3D model (16,22) of neutral wind. The calculation was carried out for different heights of combustion: 80 and 100 km (maximal heights of meteors burning at night and day for detected lifetime (0.1-40sec) [Crain(1963)]). The statistics was made over the full range of dates, including not only meteor showers, but also meteorically calm days. The accumulation time necessary for one measurement of the wind velocity vector was 1 hour. For the rejection of very calm hours and the meteor observations strongly localized over the azimuths, we limited the hours in which the calculations can be made. Measurement of wind speed at a given hour was considered correct under the following conditions: the number of recorded meteors should exceed 10 meteors per hour, the azimuthal coverage by meteor trail observations in the radar field-of-view should be at least 2 beams (6-10 degrees) during the hour.

Using obtained wind velocities in the two models, the horizontal wind roses were constructed (the median value of the horizontal projection of the wind speed for the selected direction of the wind) with azimuthal resolution 15° . Wind roses are shown in Fig.8. From Fig.8A,B one can see that the roses change slightly with the burning height. From Fig.8C,D one can see that qualitatively the wind roses calculated in 2D and 3D models are close to each other, and demonstrate the prevalence of the zonal wind over the meridional, which does not contradict the existing data [Rüfenacht et al.(2016)]. At the same time, the median values of the zonal wind in both models are close, while the meridional wind within 3D model is 2-3 times higher than the meridional wind in 2D model(Fig.8E,F). This indicates the prevalence of the zonal wind over the vertical wind, which suggests the validity of the proposed method of wind recovery from the EKB ISTP SB RAS meteor trail data.

6 Discussion and conclusion

In the paper we describe the algorithms for interpreting the signals scattered on meteor trails and used at EKB ISTP SB RAS radar. The algorithm is divided into two phases - the detection of underdense meteor trail echo and the estimation of its parameters. At the first phase, spatially localized bursts of amplitude above the average signal level, monotonically decaying in time are detected. In the second phase, the quadrature components of the scattered signal are approximated by the exponential model with Doppler shift by the method of least squares, by performing additional filtering of the found meteor trails based on the resulting accuracy of phase and amplitude approximation. In general, the

algorithm is similar to the algorithms used for specialized meteor radars, but when restoring the scattering parameters it approximates the quadrature components of the received signal by the model instead of separate approximating the amplitude and the phase of the signal.

To test the algorithm, it was shown that, on the day of the maximum of the Geminid shower 13.12.2016, the scattering detected by the algorithm has an aspect sensitive character and correspond to scattering at irregularities elongated with the direction toward the radiant of the meteor shower. This confirms that the source of signals detected by the algorithm is scattering on meteor trails.

In the paper, the solution is presented for reconstructing the vector of the neutral wind velocity from the obtained data by the weighted least-squares method under the assumption of the isotropy of the field of neutral winds in the local coordinate system of the meteors. Based on geometric considerations and assuming a Gaussian distribution of the meteor trail heights the weight function was found and the inversion technique was implemented at EKB radar.

To test the inversion technique the neutral winds were reconstructed in the models of two-dimensional (horizontal) wind and three-dimensional wind based on the EKB radar long-term measurements (from 23.12.2016 to 03.07.2017). The roses of the horizontal neutral winds obtained in both models are compared, their proximity and the expected predominance of the zonal wind over the meridional one are shown. The comparison showed that statistically the vertical wind is smaller than the zonal wind.

The developed algorithms allow processing the scattered signals in real time. The algorithm for detecting the meteor trails and estimating their parameters (the Doppler shift and the lifetime), has been put into regular operation at the EKB ISTP SB RAS radar.

Acknowledgements

In the paper the data from EKB ISTP SB RAS radar were used. The work was supported by FSR program II.12.2.3.

References

- [Arnold et al.(2003)] Arnold, N.F., Cook, P.A., Robinson, T., Lester, M., Chapman, P.J., Mitchell, N., 2003. Comparison of D-region Doppler drift winds measured by the SuperDARN Finland HF radar over an annual cycle using the Kiruna VHF meteor radar. *Annales Geophysicae* V.21, pp.2073–2082. DOI:10.5194/angeo-21-2073-2003.
- [Berngardt et al.(2013)] Berngardt, O., Kurkin, V., Zhrebtssov, G., Grigorieva, S., Kusonski, O., 2013. Ionospheric effects during first 2 hours after the 'Chelyabinsk' meteorite impact (in russian). *Solar-Terrestrial physics* V.24, pp.3–14.
- [Berngardt et al.(2017)] Berngardt, O., Lebedev, V., Kutelev, K., Kushnarev, D., Grkovich, K., 2017. First joint observations of radioaurora by ultrashort wave and shortwave ISTP SB RAS radars. *Izvestiya VUZov. Radiofizika* (in russian, in press) V.LX, pp.n/a.

- [Berngardt et al.(2015)] Berngardt, O.I., Voronov, A.L., Grkovich, K.V., 2015. Optimal signals of Golomb ruler class for spectral measurements at EKB SuperDARN radar: Theory and experiment. *Radio Science* V.50, pp.486–500. DOI:10.1002/2014RS005589.
- [Briczinski et al.(2009)] Briczinski, S.J., Mathews, J.D., Meisel, D.D., 2009. Statistical and fragmentation properties of the micrometeoroid flux observed at Arecibo. *Journal of Geophysical Research: Space Physics* V.114, pp.A04311. DOI:10.1029/2009JA014054.
- [Campbell-Brown(2008)] Campbell-Brown, M.D., 2008. High resolution radiant distribution and orbits of sporadic radar meteoroids. *Icarus* V.196, pp.144 – 163. DOI:https://doi.org/10.1016/j.icarus.2008.02.022.
- [Close et al.(2002)] Close, S., M. Hunt, S., M. McKeen, F., J. Minardi, M., 2002. Characterization of Leonid meteor head echo data collected using the VHF-UHF Advanced Research Projects Agency Long-Range Tracking and Instrumentation Radar (ALTAIR). *Radio Science* V.37, pp.9–1.
- [Crain(1963)] Crain, C.M., 1963. Decay of ionization impulses in the D and E regions of the ionosphere. *Journal of Geophysical Research* V.68, pp.2167–2169. DOI:10.1029/jz068i008p02167.
- [Deegan et al.(1970)] Deegan, N., Fitzpatrick, R., Forti, G., Grossi, M., Schaffner, M., Southworth, R., Ma., S.A.O.C., 1970. Study of meteor wind measurement techniques. N.1, Publisher:Defense Technical Information Center.
- [Erickson et al.(2001)] Erickson, P.J., Lind, F.D., Wendelken, S.M., Faubert, M.A., 2001. Meteor head echo observations using the Millstone Hill UHF incoherent scatter radar system, in: editor:Warmbein, B. (Ed.), *Meteoroids 2001 Conference*, pp. pp.457–463.
- [Hall et al.(2006)] Hall, C., Aso, T., Tsutsumi, M., Nozawa, S., Meek, C., Manson, A., 2006. Comparison of meteor and medium frequency radar kilometer scale {MLT} dynamics at 70N. *Journal of Atmospheric and Solar-Terrestrial Physics* V.68, pp.309 – 316. DOI:10.1016/j.jastp.2005.03.025.
- [Hall et al.(1997)] Hall, G., MacDougall, J., Moorcroft, D., St.-Maurice, J.P., Manson, A., Meek, C., 1997. Super Dual Auroral Radar Network observations of meteor echoes. *J. Geophys. Res.* V.102, pp.14603–14614. DOI:10.1029/97JA00517.
- [IMO(2015)] IMO, 2015. 2016 Meteor Shower Calendar. International Meteor Organization.
- [Janches et al.(2009)] Janches, D., Dyrud, L.P., Broadley, S.L., Plane, J.M.C., 2009. First observation of micrometeoroid differential ablation in the atmosphere. *Geophysical Research Letters* V.36, pp.L06101. DOI:10.1029/2009GL037389.
- [Jenkins and Jarvis(1999)] Jenkins, B., Jarvis, M.J., 1999. Mesospheric winds derived from SuperDARN HF radar meteor echoes at Halley, Antarctica. *Earth, Planets and Space* V.51, pp.685–689. DOI:10.1186/BF03353226.

- [Jenkins et al.(1998)] Jenkins, B., Jarvis, M.J., Forbes, D.M., 1998. Mesospheric wind observations derived from Super Dual Auroral Radar Network (SuperDARN) HF radar meteor echoes at Halley, Antarctica: Preliminary results. *Radio Sci.* V.33, pp.957–965. DOI:10.1029/98rs01113.
- [Jones et al.(2005)] Jones, J., Brown, P., Ellis, K.J., Webster, A.R., Campbell-Brown, M., Krzemenski, Z., Weryk, R.J., 2005. The Canadian Meteor Orbit Radar: system overview and preliminary results. *Planetary Space Science* V.53, pp.413–421. DOI:10.1016/j.pss.2004.11.002.
- [Jones and Jones(1990)] Jones, W., Jones, J., 1990. Ionic diffusion in meteor trains. *Journal of Atmospheric and Terrestrial Physics* V.52, pp.185–191. DOI:10.1016/0021-9169(90)90122-4.
- [Kero et al.(2012)] Kero, J., Szasz, C., Nakamura, T., Meisel, D.D., Ueda, M., Fujiwara, Y., Terasawa, T., Nishimura, K., Watanabe, J., 2012. The 20092010 MU radar head echo observation programme for sporadic and shower meteors: radiant densities and diurnal rates. *Monthly Notices of the Royal Astronomical Society* V.425, pp.135–146. DOI:10.1111/j.1365-2966.2012.21407.x.
- [Lester et al.(2004)] Lester, M., Chapman, P.J., Cowley, S.W.H., Crooks, S.J., Davies, J.A., Hamadyk, P., McWilliams, K.A., Milan, S.E., Parsons, M.J., Payne, D.B., Thomas, E.C., Thornhill, J.D., Wade, N.M., Yeoman, T.K., Barnes, R.J., 2004. Stereo CUTLASS - A new capability for the SuperDARN HF radars. *Annales Geophysicae* V.22, pp.459–473. <https://www.ann-geophys.net/22/459/2004/>, DOI:10.5194/angeo-22-459-2004.
- [Lovell(1954)] Lovell, A.C.B., 1954. *Meteor Astronomy*. Publisher:Oxford At The Clarendon Press.
- [Manning et al.(1954)Manning, Peterson and Villard] Manning, L.A., Peterson, A.M., Villard, O.G., 1954. Ionospheric wind analysis by meteoric echo techniques. *Journal of Geophysical Research* V.59, pp.47–62. DOI:10.1029/JZ059i001p00047.
- [Mathews et al.(2010)] Mathews, J., Briczinski, S.J., Malhotra, A., Cross, J., 2010. Extensive meteoroid fragmentation in V/UHF radar meteor observations at Arecibo Observatory. *Geophysical Research Letters* V.37, pp.L04103. DOI:10.1029/2009gl041967.
- [Mathews et al.(2003)] Mathews, J., Doherty, J., Wen, C.H., Briczinski, S., Janches, D., Meisel, D., 2003. An update on UHF radar meteor observations and associated signal processing techniques at Arecibo Observatory. *Journal of Atmospheric and Solar-Terrestrial Physics* V.65, pp.1139 – 1149. DOI:10.1016/j.jastp.2003.07.009.
- [McKinley(1961)] McKinley, D.W.R., 1961. *Meteor Science and Engineering*. Publisher:McGraw-Hill Book Company,Inc.
- [Nakamura et al.(1991)] Nakamura, T., Tsuda, T., Tsutsumi, M., Kita, K., Uehara, T., Kato, S., Fukao, S., 1991. Meteor wind observations with the MU radar. *Radio Science* V.26, pp.857–869. DOI:10.1029/91RS01164.

- [Parris(2003)] Parris, R.T., 2003. Design and Implementation of a Meteor Tracking Retrofit for the HF Radar at Kodiak Island, Alaska. Master's thesis. University of Alaska Fairbanks.
- [Ribeiro et al.(2013)] Ribeiro, A.J., Ruohoniemi, J., Ponomarenko, P., N. Clausen, L.B., Baker, J., Greenwald, R., Oksavik, K., de Larquier, S., 2013. A comparison of SuperDARN ACF fitting methods. *Radio Science* V.48, pp.274–282. DOI:10.1002/rds.20031.
- [Rüfenacht et al.(2016)] Rüfenacht, R., Hocke, K., Kämpfer, N., 2016. First continuous ground-based observations of long period oscillations in the vertically resolved wind field of the stratosphere and mesosphere. *Atmospheric Chemistry & Physics* V.16, pp.4915–4925. DOI:10.5194/acp-16-4915-2016.
- [Szasz et al.(2008)] Szasz, C., Kero, J., Meisel, D.D., Pellinen-Wannberg, A., Wannberg, G., Westman, A., 2008. Orbit characteristics of the tristatic EISCAT UHF meteors. *Monthly Notices of the Royal Astronomical Society* V.388, pp.15. DOI:10.1111/j.1365-2966.2008.13374.x.
- [Thomas et al.(1988)] Thomas, R.M., Whitham, P.S., Elford, W.G., 1988. Response of high frequency radar to meteor backscatter. *Journal of Atmospheric and Terrestrial Physics* V.50, pp.703–724. DOI:10.1016/0021-9169(88)90034-7.
- [Tsutsumi et al.(1999)] Tsutsumi, M., Holdsworth, D., Nakamura, T., Reid, I., 1999. Meteor observations with an MF radar. *Earth, Planets and Space* V.51, pp.691–699. DOI:10.1186/BF03353227.
- [Yukimatu and Tsutsumi(2003)] Yukimatu, A., Tsutsumi, M., 2003. Correction to 'A new SuperDARN meteor wind measurement: Raw time series analysis method and its application to mesopause region dynamics'. *Geophys. Res. Lett.* V.30, pp.1026. DOI:10.1029/2002gl016560.
- [Zhu et al.(2016)] Zhu, Q., Dinsmore, R., Gao, B., Mathews, J., 2016. High-resolution radar observations of meteoroid fragmentation and flaring at the Jicamarca Radio Observatory. *Monthly Notices of the Royal Astronomical Society* V.457, pp.1759–1769. DOI:10.1093/mnras/stw070.

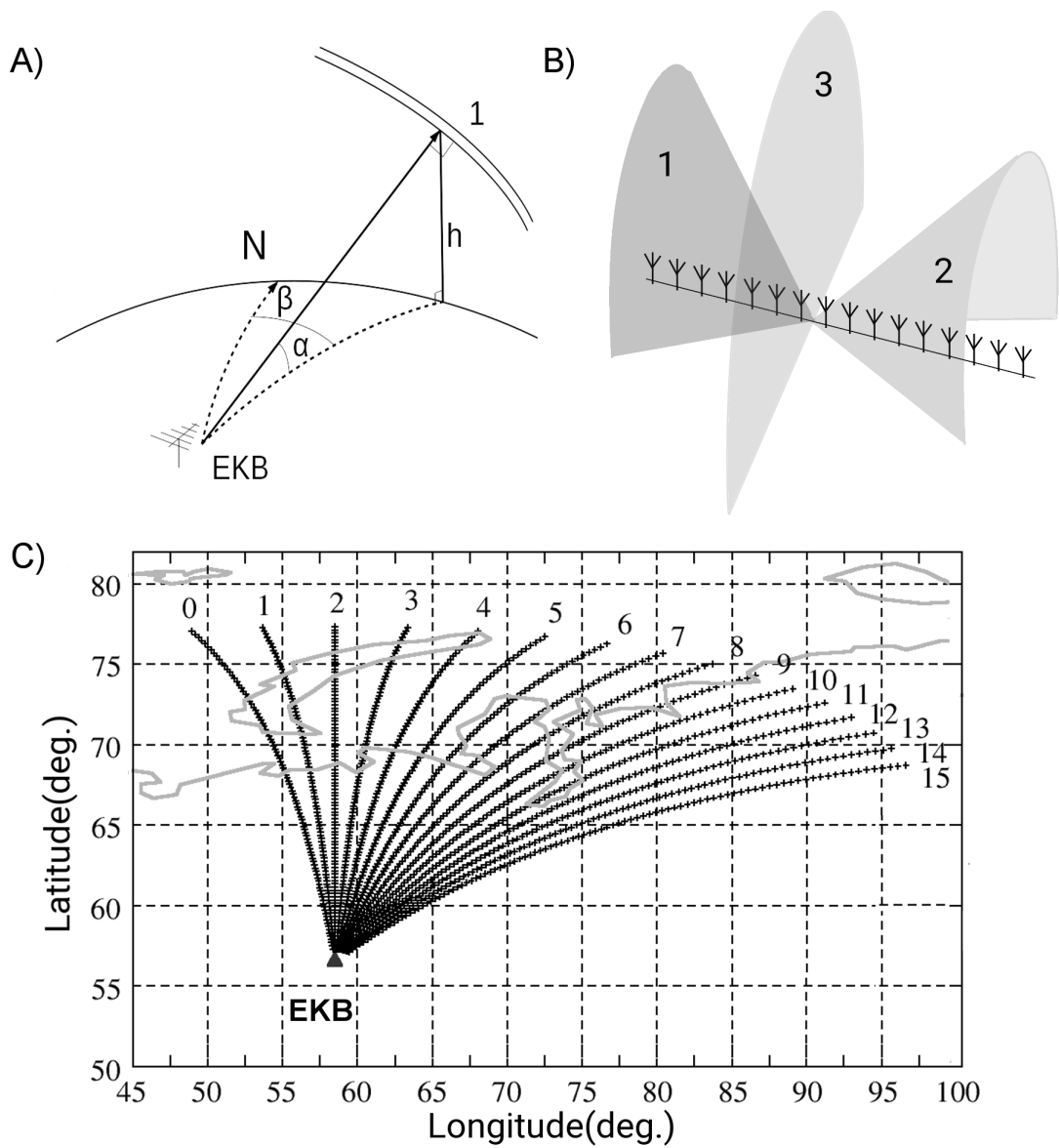


Figure 1: A) - scheme of scattering at the meteor trail (1). B) - antenna pattern surfaces for EKB radar: (1) and (2) - for the cases of outer beams (beams 0 and 15), (3) - for the case of central beams (beams 7 and 8); C) - field of view of EKB radar.

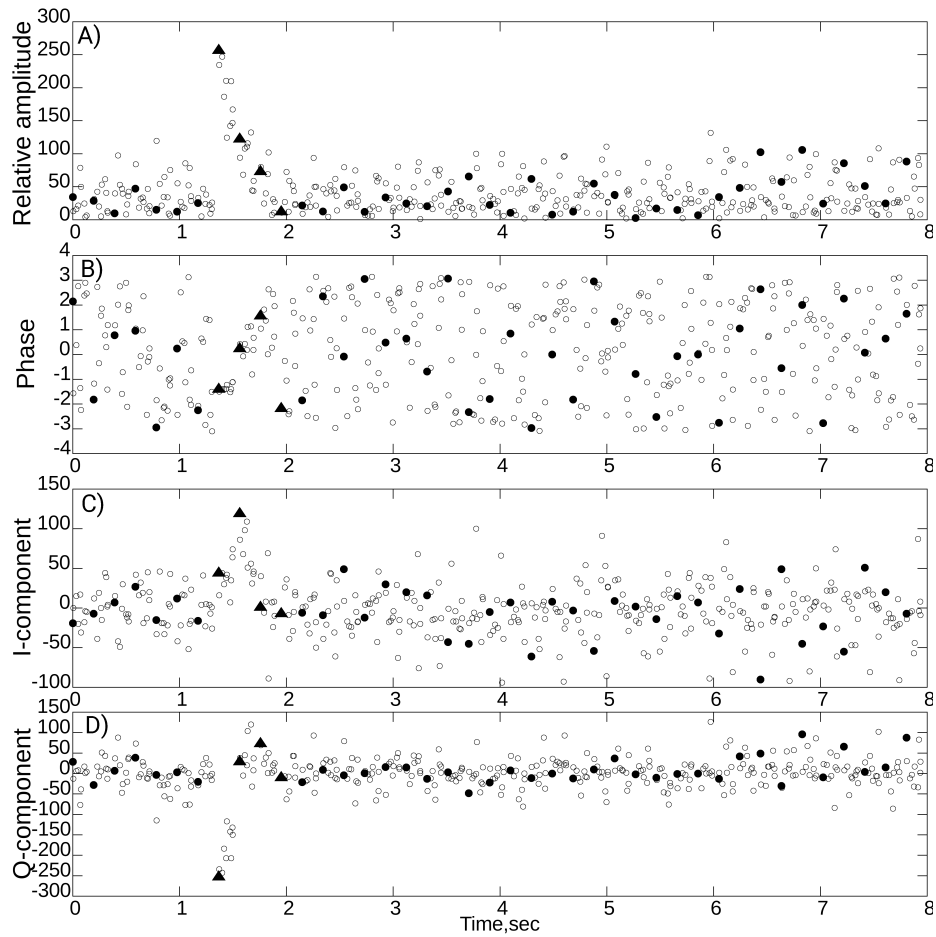


Figure 2: Example of the amplitude (A), phase (B) and quadrature components (C, D) of the signal at a fixed range R_k in the presence of meteor trail scatter. Black triangles denote the first pulses of the sounding sequences identified in the framework of stage 1, black circles - the first pulses of the remaining sequences within the scanning cycle, circles denote the signal from all other sounding pulses.

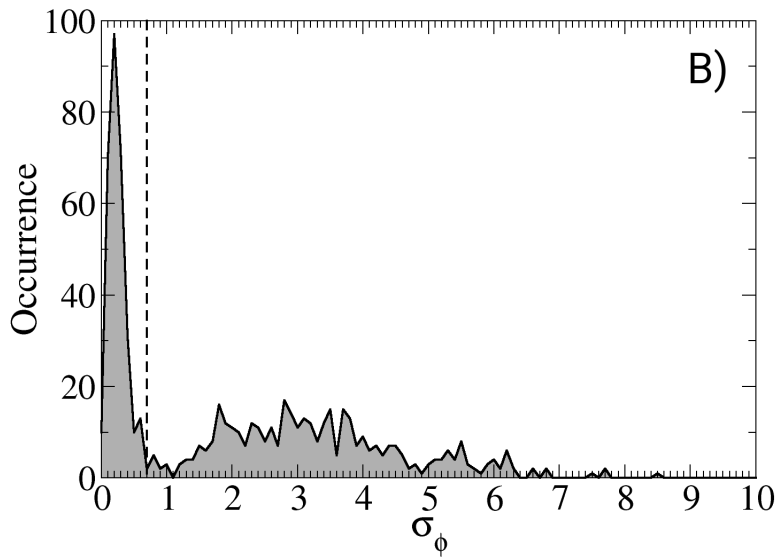
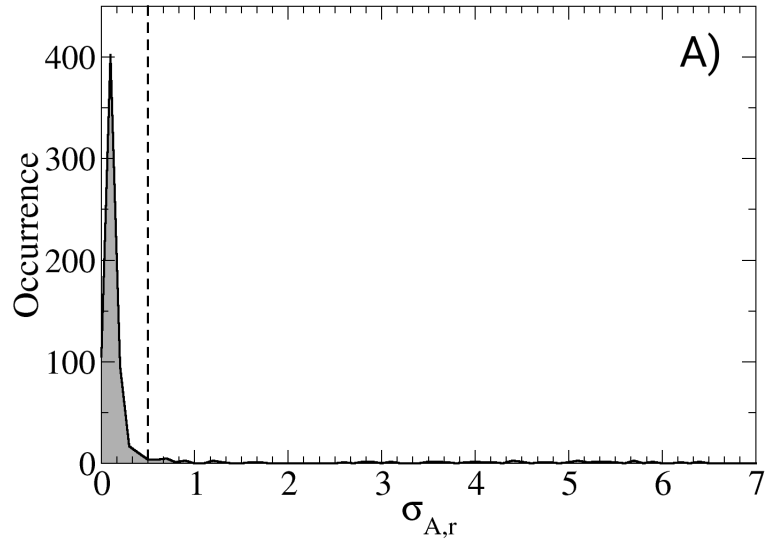


Figure 3: Distributions of the errors between experimental and model values. A) normalized error of amplitude estimation $\sigma_{A,r}(\omega, \tau)$, B) error of the phase estimation $\sigma_\phi(\omega, \tau)$. The dashed lines correspond to the threshold values.

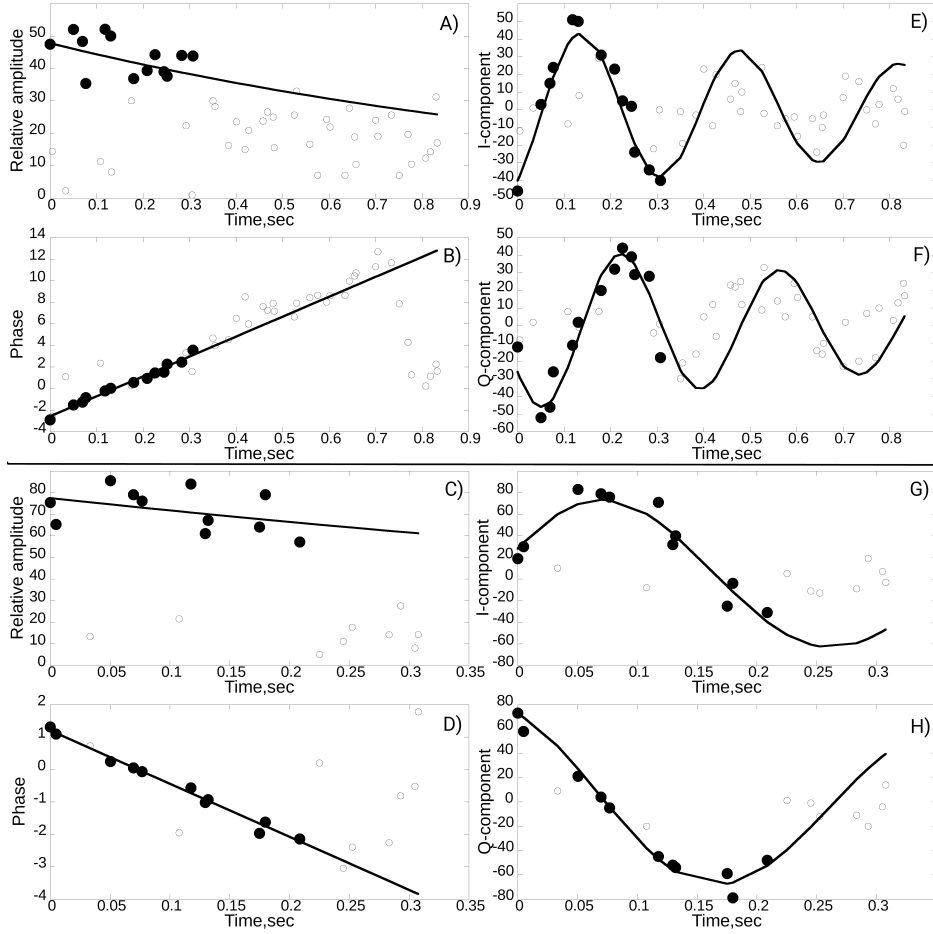


Figure 4: Two examples of well-fitted meteor trail echo. A), C) are the amplitude modulus of the signal $|u(t_i)|$; B), D) are the phases of the signal $\arg(u(t_i))$; E-H) - I/Q signal components. The black circles are the experimental signal, the empty circles are the noisy values. The lines correspond to the model approximation.

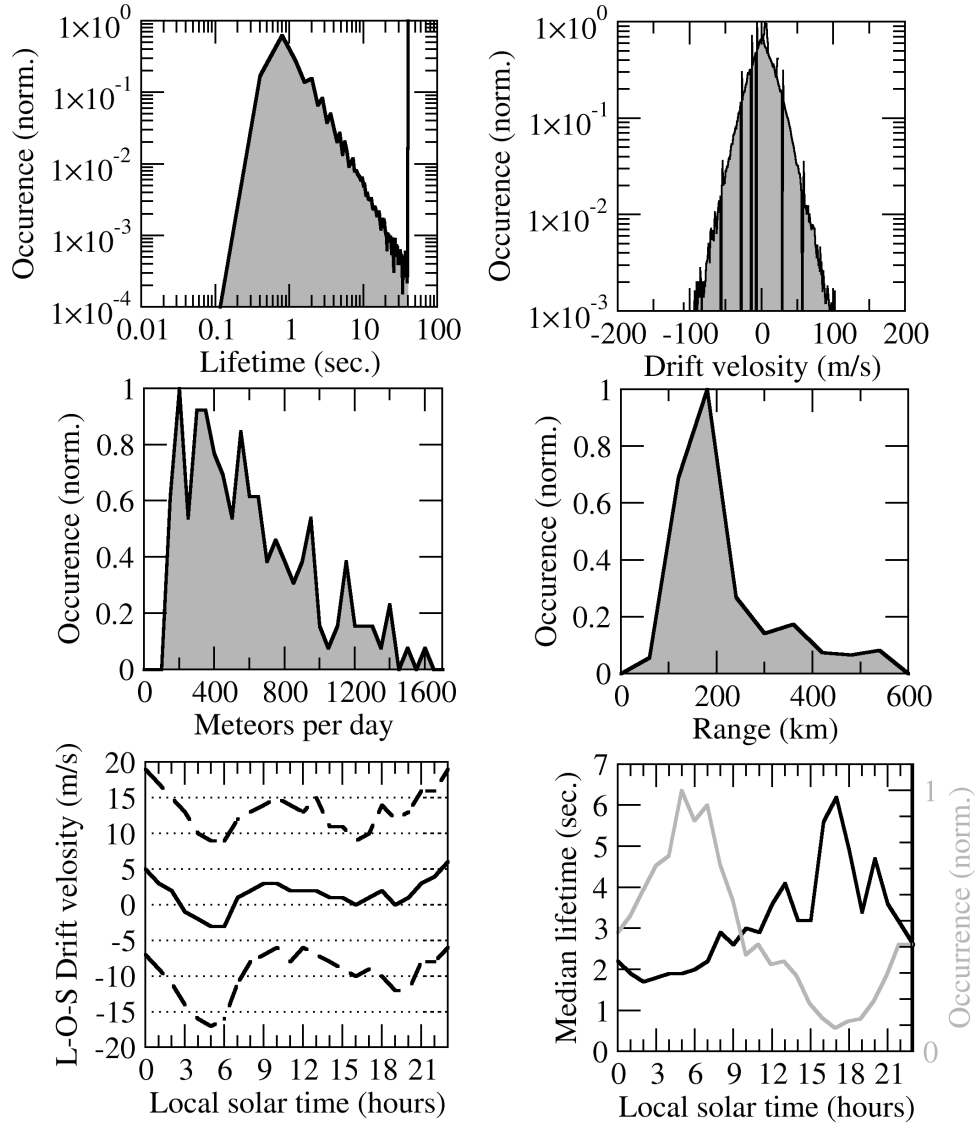


Figure 5: Statistics of meteor trail observations at EKB radar from December 2016 to August 2017. A) - meteor trails number as function of their lifetime B) - the meteor trails number as function of their line-of-sight Doppler velocity; C) - distribution of the daily number of meteor trails; D) - distribution of the meteor trails as a function of radar range; E) - median line-of-sight velocity (black line) and its first and third quartiles (green lines), as a function of local solar time; F) - the median lifetime of the meteor trail as a function of local solar time (black line), normalized distribution of meteor trails as a function of local solar time (grey line)

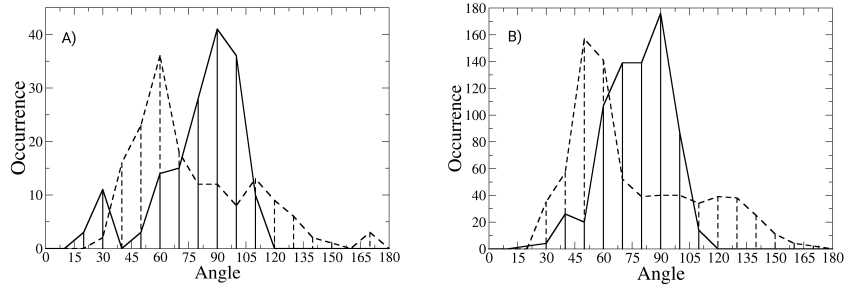


Figure 6: Distributions of aspect angles between the direction to the meteor shower radiant from scattering point and direction to the scattering point from the radar. A) - 1st channel, B) - 2nd channel. The solid line is the distribution under approximation of the scattering in the main antenna lobe, the dashed line is the distribution under approximation of the scattering in the back lobe.

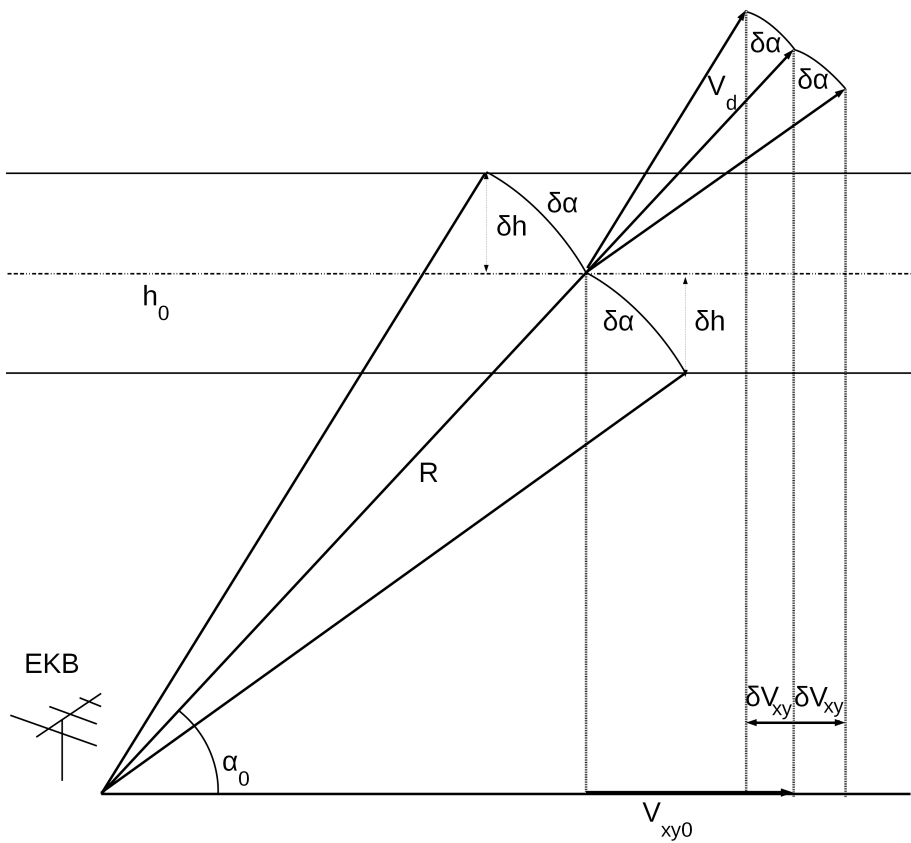


Figure 7: Geometry for the calculation of $W(R_i)$.

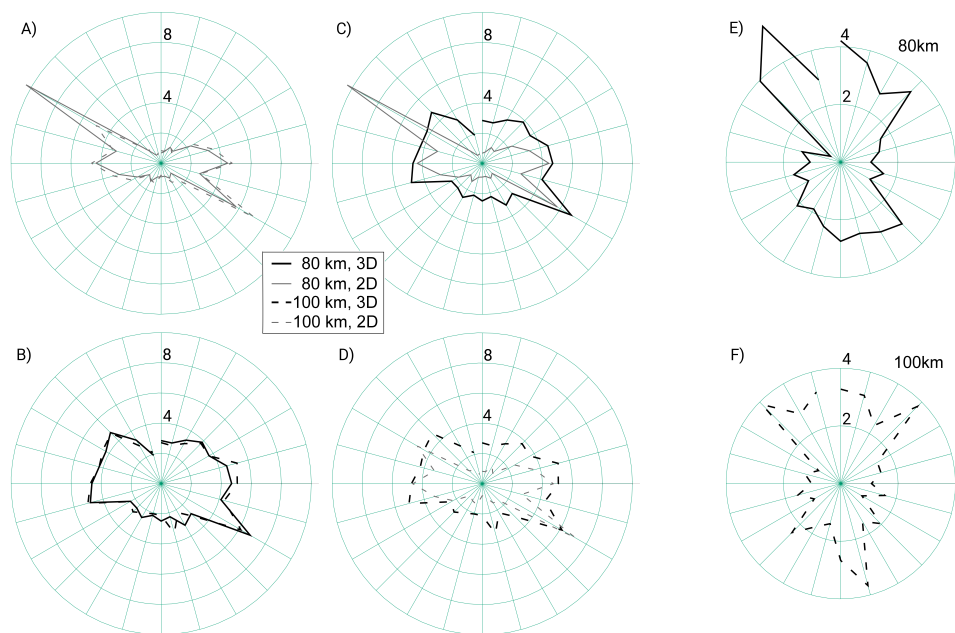


Figure 8: Comparison of wind roses obtained for different wind models (3D and 2D) and different meteor trail heights. A) - 2D wind model, grey solid line corresponds to 80 km height, grey dashed line corresponds to 100 km height, (in m/s); B) - 3D wind model, black solid line corresponds to 80 km height, black dashed line corresponds to 100 km height (in m/s); C) - comparison of 3d and 2D models at 80km height: black solid line - 3D model, grey solid line - 2D model (in m/s); D) - comparison of 3d and 2D models at 100km height: black dashed line - 3D model, grey dashed line - 2D model (in m/s); E) - relationship between rose in 3D model to rose in 2D model for height 80km ; F) - relationship between rose in 3D model to rose in 2D model for height 100km